



Novel amorphous mesoporous $0.25\text{Cr}_2\text{O}_3-0.75\text{ZrO}_2$ nanomaterials synthesized by a surfactant-assisted hydrothermal method for ethanol oxidation



Hala R. Mahmoud

Department of Chemistry, Faculty of Education, Ain Shams University, Roxy, 11757, Cairo, Egypt

ARTICLE INFO

Article history:

Received 29 February 2016

Received in revised form

16 June 2016

Accepted 26 June 2016

Available online 28 June 2016

Keywords:

Amorphous materials

Nanostructured materials

Precipitation

Catalysis

Optical properties

Transmission electron microscopy

TEM

ABSTRACT

Novel mesoporous $0.25\text{Cr}_2\text{O}_3-0.75\text{ZrO}_2$ nanomaterials were successfully synthesized via hydrothermal method in the presence of anionic, cationic and non-ionic surfactants, namely, SDS, CTAB and Triton X-100, respectively. The effect of different surfactants and their concentrations on the physicochemical properties and the catalytic activity of the catalysts were studied by the XRD, HR-TEM, FT-IR, BET, UV–vis/DR, NH_3 -TPD and ethanol oxidation techniques. XRD results indicated that all the as-prepared nanomaterials were amorphous materials. The morphology study demonstrated that the sample with CTAB has the smallest particle size while that with SDS has the largest value. The catalysts prepared with non-ionic and cationic surfactants have the highest surface area and the pore volume while those prepared with anionic or without surfactant have the smallest values. Additionally, the surface area of the catalysts decreases with increasing the surfactant content. The optical study indicated that the absorption peak of the nanomaterials shifts towards the short wavelength by changing the various surfactants. It is well-observed by NH_3 -TPD that the non-ionic and cationic surfactants enhanced the amount of acidic sites on the catalyst surface. These results indicate that the catalytic activity of mesoporous catalysts can be improved effectively by the addition of non-ionic and cationic surfactants.

© 2016 Elsevier B.V. All rights reserved.

1. Introduction

Nanotechnology involves the study of the synthesis, characterization, and properties of nanomaterials [1]. The emergence of nanotechnology has led to innovations in many areas of electronics, energy management, structural materials, construction, information technology, pharmaceuticals, and medical devices. The largest share of the manufacturing and application market among the different nanomaterials belongs to metal oxide nanomaterials [2]. Transition metal oxide nanoparticles represent a broad class of materials that have been investigated extensively due to their interesting catalytic, electronic, and magnetic properties relative to those of the bulk counterparts, and the wide scope of their potential applications [3,4]. Among these materials, chromium oxides have attracted much attention recently because of their importance both in science and technology [5]. Special attention has been focused on the formation and properties of chromia (Cr_2O_3), which is important in specific applied applications such as in green

pigments [6], ceramic coatings [7], gas sensors [8], catalysts [9], antitumor applications [10] and solar energy application [11]. As well as, zirconia has been widely studied because of its attractive technological properties, including high thermal and chemical stability, good mechanical strength and wear resistance, excellent dielectric properties and good ion-exchange properties [12]. Due to their prominent physical and chemical properties, zirconia (ZrO_2) ceramic materials have been widely used in modern engineering and industry fields, such as chemical sensors [13], magnetic materials [14], thermal barrier coatings [15], refractory materials [16], catalysts [17] and biomedical applications [18].

Since the size and morphologies of nanomaterials have significant influence on their properties, many efforts have been devoted to fabricate nanostructured materials [19,20]. As we know, surfactant is widely used as additive to control the structure and morphologies of conducting polymers and inorganic species [21,22]. The surface active agents, or also known as surfactants were molecules that have tendency to adsorb at the surfaces and interfaces. They have a dual chemical structure, one part of the molecule is hydrophilic and the other is hydrophobic. Surfactant with amphiphilic character adsorb on the interface to reduce the free energy of

E-mail addresses: halamahmoud2@yahoo.com, halarashaad@edu.asu.edu.eg.

phase boundary [23].

Catalytic technologies are critical to present and future energy, chemical process, and environmental industries [24]. For instance, catalytic conversion of alcohol over metal oxides into hydrocarbons is useful for petrochemical raw materials or as a motor fuel [25]. Ethanol dehydration with diethyl ether (DEE) and/or ethylene formation occurs lightly on acid heterogeneous catalysts [26]. Furthermore, the ethylene is one of the major feedstock of the petrochemical industry.

Nevertheless, to the best of our knowledge, the systematic investigation of the effects of different types of surfactants (anionic, cationic and non-ionic) on the mesoporous $0.25\text{Cr}_2\text{O}_3$ – 0.75ZrO_2 binary oxide catalyst for ethanol oxidation has not been reported. To improve the performance of the as-prepared mesoporous catalysts, it is essential to make insight into the characteristics with different surfactants. Continuing my previous work [27], herein, three kinds of surfactants with two different concentrations, that is, SDS (anionic), CTAB (cationic), and Triton X-100 (non-ionic), were used as surfactants to prepare $0.25\text{Cr}_2\text{O}_3$ – 0.75ZrO_2 nanomaterials via hydrothermal process. As well as the effect of different surfactants on the structural, optical, acidity and catalytic properties of the corresponding novel mesoporous $0.25\text{Cr}_2\text{O}_3$ – 0.75ZrO_2 catalysts were characterized by X-ray diffraction (XRD), high-resolution transmission electron microscopy (HR-TEM), energy dispersive spectroscopic (EDS), Fourier transform infrared spectroscopy (FT-IR), N_2 adsorption–desorption measurements (BET), UV–visible diffuse reflectance spectroscopy (UV–vis/DR), temperature-programmed desorption profile of NH_3 (NH_3 -TPD) and the oxidation of ethanol.

2. Experimental

2.1. Materials

All the chemicals in this work were of analytical grade and used as received without further purification. The water used throughout all experiments was well purified. $\text{Cr}(\text{NO}_3)_3 \cdot 9\text{H}_2\text{O}$ (Oxford) as chromia source; $\text{ZrOCl}_2 \cdot 8\text{H}_2\text{O}$ (Oxford) as zirconia source; ammonium hydroxide (NH_4OH) (Alpha); ethanol (absolute) (for HPLC, $\geq 99\%$) and acetylacetone (acac) (99% purity). Sodium dodecyl sulfate (SDS, $\text{CH}_3(\text{CH}_2)_{11}\text{SO}_4\text{Na}$) (Oxford), cetyltrimethylammonium bromide (CTAB, $\text{CH}_3(\text{CH}_2)_{15}\text{N}(\text{CH}_3)_3\text{Br}$) (BDH), and T-octylphenoxypoly-ethoxyethanol (Triton X-100) ($\text{TX}-100$, $\text{C}_{34}\text{H}_{62}\text{O}_{11}$) (Merck) were used as cationic, anionic and non-ionic surfactants.

2.2. Catalyst preparation

Mesoporous $0.25\text{Cr}_2\text{O}_3$ – 0.75ZrO_2 catalyst synthesized at 210°C for 3 h (CZ-H213), which had the highest ethanol conversion and ethylene production among $0.25\text{Cr}_2\text{O}_3$ – 0.75ZrO_2 binary oxide catalysts [27], were prepared by hydrothermal method. $0.25\text{Cr}_2\text{O}_3$ – 0.75ZrO_2 nanomaterials were prepared in this work using the method of surfactant-assisted hydrothermal. Three different surfactants were used to synthesize the catalysts as following steps.

2.2.1. Catalyst preparation by anionic surfactant

In brief, the $0.25\text{Cr}_2\text{O}_3$ – 0.75ZrO_2 nanomaterials were prepared by adding an aqueous solution containing two different concentrations of SDS (0.1 and 0.6 M), 9 mL acetylacetone (acac), and 30 mL of ethanol to a mixed aqueous solution of $\text{Cr}(\text{NO}_3)_3 \cdot 9\text{H}_2\text{O}$ and $\text{ZrOCl}_2 \cdot 8\text{H}_2\text{O}$ ($[\text{Cr}] + [\text{Zr}] = 1.0$ M).

2.2.2. Catalyst preparation by cationic and non-ionic surfactants

In a typical synthetic route, the $0.25\text{Cr}_2\text{O}_3$ – 0.75ZrO_2 nanomaterials were prepared by adding an aqueous solution containing two different concentrations of CTAB and TX-100 (0.1 and 0.6 M) to a mixed aqueous solution of $\text{Cr}(\text{NO}_3)_3 \cdot 9\text{H}_2\text{O}$ and $\text{ZrOCl}_2 \cdot 8\text{H}_2\text{O}$ ($[\text{Cr}] + [\text{Zr}] = 1.0$ M).

Finally, the three different mixtures were stirred for 30 min and then aqueous ammonia (2.0 M) was slowly added with vigorous stirring till the pH was 10. The above mixtures were stirred for another 90 min, and then transferred into a stainless Teflon-lined 100 mL capacity autoclave at 210°C for 3 h. After this time, the autoclave was quenched to room temperature and the resulting precipitate was centrifuged and washed repeatedly with doubly distilled water to remove the free surfactant, products were heated at 50°C for several hours to remove water. In order to describe simply, the final products were denoted as CZ- H_{XY} , in which (X = S, C or T refers to SDS, CTAB or TX-100) and (Y = 0.1 or 0.6 M refers to surfactant concentration). The mesoporous $0.25\text{Cr}_2\text{O}_3$ – 0.75ZrO_2 catalyst which was hydrothermally synthesized previously [27] at 210°C for 3 h (CZ-H213) surfactant-free using for comparison.

2.3. Catalyst characterization

X-ray diffraction powder patterns were recorded at room temperature on a Philips Xpert powder diffractometer, using the Bragg–Brentano configuration and the $\text{CuK}\alpha$, radiation $\lambda = 1.5406$ Å. The morphology of the catalysts was observed by high-resolution transmission electron microscope (HR-TEM) equipped with energy dispersive spectroscopic (EDS) microanalysis system (JEM-2100CX (JEOL)). Fourier transform infrared spectroscopy (FT-IR) was recorded on a Jasco IR 4100 spectrometer (Japan) using KBr pellets. The textural characteristics of the mesoporous catalysts were determined using a Quantachrome NOVA 2000 Autosorb Gas Sorption System instrument (USA). The surface area was calculated from adsorption–desorption of nitrogen at 77 K using the multi-point Brunauer–Emmett–Teller (BET) method. Before each N_2 sorption measurement, the samples were outgassed for 2 h at 200°C . The total pore volume, V_p was estimated to be the liquid volume of the nitrogen at a relative pressure of about 0.99. The pore size distribution and pore diameter of the catalysts were determined from desorption branch of the isotherm using Barrett, Joyner, Halenda (BJH) method. UV–visible diffuse reflectance spectroscopy (UV–vis/DR) was carried out on JASCO V-550 spectrometer (Japan) equipped with an integrating sphere accessory for diffuse reflectance spectra. Barium sulfate was used as a reference. The temperature-programmed desorption profile of NH_3 (NH_3 -TPD) study was performed on a BELCAT-B catalyst analyzer with TCD detector (Japan). The catalyst was put in the cell and heated in helium atmosphere at 500°C for 3 h. After cooling the catalyst to room temperature the NH_3 was passed (10% in He gas) with flow rate 30 ml/min for 1 h to saturate acid sites of the catalyst. Afterwards the TPD experiment was carried out by purging helium with a rate of 30 mL/min from 25 to 900°C with a temperature ramp at $5^\circ\text{C}/\text{min}$.

2.4. Catalytic activity test

The catalytic oxidation of ethanol was performed in a fixed-bed flow reactor at atmospheric pressure. Typically, 100 mg sample was placed in a Pyrex glass reactor tube (10 mm i.d.). Argon gas was used as a carrier and the ethanol vapor was introduced into the reactor through an evaporator/saturator at the ethanol pressure equal 100 Torr with a flow rate of 30 ml/min. Before every run the catalyst sample was activated by heating at 300°C in a current of argon for 1 h then cooled to the catalytic reaction temperature. The

steady-state tests were conducted isothermally every 25 °C from 150 °C to 400 °C and the gas products were analyzed by a flame ionization detection (FID) of Perkin-Elmer Auto System XL Gas Chromatograph (GC) equipped with a packed column (10% squalane supported on chromosorb, 4 m). The temperature of the detector was 250 °C and the column temperature was programmed at 60 °C.

3. Results and discussion

3.1. Structural characterization (XRD, HR-TEM, FT-IR, BET)

The XRD patterns of 0.25Cr₂O₃–0.75ZrO₂ binary oxide catalysts synthesized using SDS, CTAB and Triton X-100 as surfactants with two different contents were displayed in Fig. 1. According to the results, no characteristic peaks were observed, meaning that all prepared nanomaterials were amorphous materials. Several studies have reported that zirconia-based binary metal oxides at higher ZrO₂ content calcined at 500 °C were an amorphous material [28]. It has been reported that the mesoporous 0.25Cr₂O₃–0.75ZrO₂ catalyst which was hydrothermally synthesized previously [27] at 210 °C for 3 h (CZ-H213) without surfactant was totally amorphous material. It has been reported that ZrO₂ may inhibit the formation of well crystalline particles, i.e., binary oxides mostly exist in the form of microcrystals [29].

The effects of surfactants on the morphologies produced in hydrothermal synthesis of different nanomaterials were studied. Fig. 2(A–D) shows the high-resolution TEM (HR-TEM) images of the CZ-H213, CZ-HC0.1, CZ-HT0.1 and CZ-HS0.1 nanomaterials, respectively. It can be seen from Fig. 2 that the particles of all catalysts have nearly spherical shapes with weak agglomeration. The average diameters of CZ-H213, CZ-HC0.1, CZ-HT0.1 and CZ-HS0.1 nanomaterials are 1.5 nm, 0.9 nm, 1.3 nm and 2.1 nm, respectively. Furthermore, the average particle size measurements clearly indicated that the cationic surfactant, CTAB, produced the smallest particle sizes of 0.25Cr₂O₃–0.75ZrO₂ nanomaterials. On the other hand, the anionic surfactant, SDS, gave the largest sizes of 0.25Cr₂O₃–0.75ZrO₂ nanoparticles. Notably, the average particle size of the 0.25Cr₂O₃–0.75ZrO₂ catalyst prepared by hydrothermal method without surfactant, CZ-H213, (1.5 nm) is higher than the catalysts prepared with cationic and non-ionic surfactants. The surfactants can be divided into two major categories including ionic and non-ionic surfactants. These surfactants affect the morphologies of the synthesized nanoparticles. In fact for the reaction system in the presence of surfactants, the surface tension of solution is reduced due to the existence of surfactant, which reduces

the energy needed for the formation of a new solid phase [30]. In addition to, the cationic surfactants in solution can surround the nanoparticles via their positive ends to prevent these particles from being agglomerated and therefore decreasing the particle size of the nanoparticles [31]. Energy dispersive spectroscopy (EDS) was performed to further confirm the composition of the prepared nanomaterials. The EDS results of CZ-HC0.1 nanomaterial (Fig. 2E) proved the presence of chromium, zirconium and oxygen elements. The analytical results from EDS were virtually identical or very close to the nominal wt% of Cr₂O₃–ZrO₂ binary oxide catalysts (Fig. 2E inset).

FT-IR is a technique that can be used to obtain information on the chemical structures of materials. Fig. 3 shows the FT-IR spectra of the as-prepared mesoporous CZ-H213, CZ-HC0.1, CZ-HT0.1 and CZ-HS0.1 nanomaterials. It could be found that all prepared mesoporous catalysts showed broad and strong absorption bands in the range 3700–3000 cm⁻¹, centered at 3430 cm⁻¹ which characterizes the stretching vibrations of surface hydroxyl groups [17]. And that the bands at 1630 cm⁻¹ can be assigned to the bend stretching vibration of adsorbed water [17]. In addition, weak absorption bands centered at 1400 cm⁻¹ were ascribed to the M–O–M deformation vibrations [32]. Moreover, the FT-IR spectra shows two weak characteristic absorption bands at 1030 cm⁻¹ and 960 cm⁻¹, which were attributed to anti-symmetric stretching vibration of M–O–M and vibration of M–OH groups, respectively [33]. Furthermore, the infrared vibration bands around 660 cm⁻¹ and 460 cm⁻¹ were corresponded to the stretching vibration of M–O [34]. Notably, in the FT-IR spectra of the as-prepared surfactant-assisted catalysts, no typical adsorption bands in the region of 2900–2800 cm⁻¹, corresponding to the stretching modes of the surfactant hydrocarbon chain [35]. Furthermore, another doublet bands correspond to asymmetric vibrations of SO₂ at 1249 cm⁻¹ and 1219 cm⁻¹ of SDS surfactant were absent [36]. On the basis of FT-IR analyses, it can be concluded that the different three surfactants (CTAB, Triton X-100 and SDS) were completely removed from the as-prepared nanomaterials.

Some studies found that improving the texture properties of the catalyst was beneficial for improving the catalytic activity. The N₂ adsorption–desorption isotherms technique was used to determine the surface area and type of porosity for synthesized nanomaterials and the isotherms are shown in Fig. 4A. The pore size distribution was measured using BJH method and is shown in Fig. 4B. Furthermore, the textural characteristics for all nanomaterials were tabulated in Table 1. It can be seen in Fig. 4A that, all isotherms are of Type IV, which indicates that the materials are mesoporous in nature. The shape of isotherms for CZ-H213, CZ-HS0.1 and CZ-HC0.6 corresponds to H2-type hysteresis loop nevertheless the shape of isotherms for CZ-HC0.1, CZ-HT0.1 and CZ-HT0.6 corresponds to H3-type hysteresis loop [23]. The H2-type hysteresis was believed to be associated with ink-bottle-like pores, often generated by agglomerates of spherical particles of non-uniform size and arrangements [37]. Furthermore, the H3-type hysteresis is generally observed for aggregates of plate-like particles giving rise to slit-shaped pores [38].

As can be seen in Table 1, the sequence of surface areas of the nanomaterials synthesized using SDS, CTAB and Triton X-100 as surfactants with two different contents was as follows: CZ-HT0.1 (646.4 m²/g) > CZ-HC0.1 (588.4 m²/g) > CZ-HC0.6 (569.9 m²/g) > CZ-HT0.6 (557.6 m²/g) > CZ-H213 (526.6 m²/g) > CZ-HS0.1 (511.6 m²/g). In addition to these mentioned above, it could be concluded that the mesoporous catalysts prepared with non-ionic and cationic surfactants, have the highest surface area and pore volume. Nevertheless, the mesoporous catalysts prepared with anionic surfactant or without surfactant showed a decrease in BET surface area. Furthermore, increasing the surfactant content

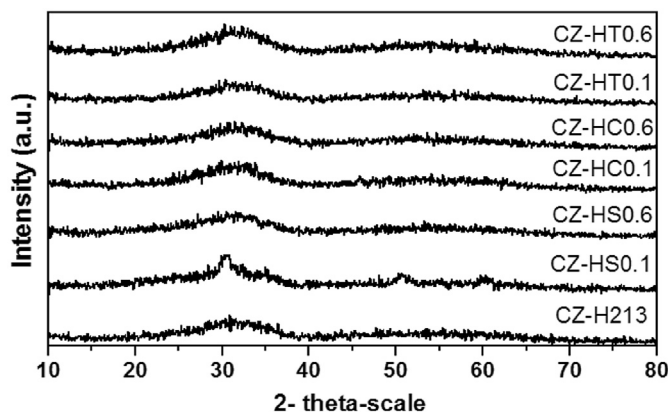


Fig. 1. XRD patterns of 0.25Cr₂O₃–0.75ZrO₂ nanomaterials synthesized in the absence and presence of surfactants (SDS, CTAB and Triton X-100).

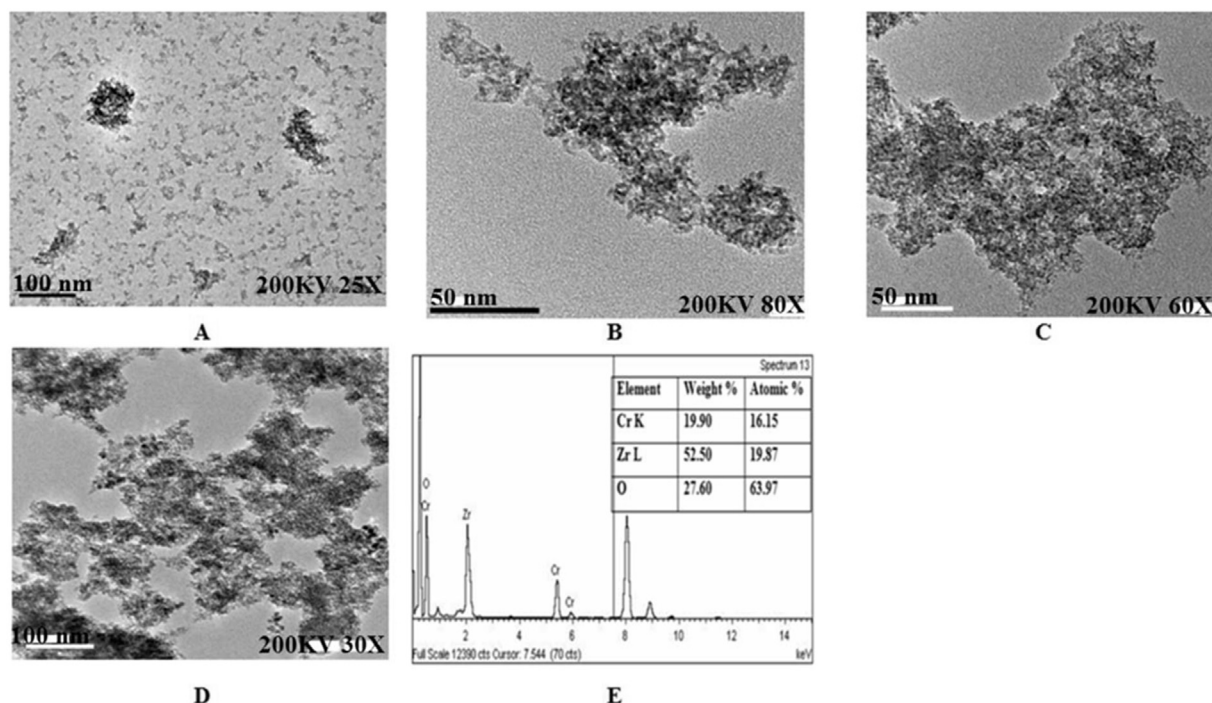


Fig. 2. HR-TEM images of (A) CZ-H213, (B) CZ-HC0.1, (C) CZ-HT0.1, (D) CZ-HS0.1, (E) EDS of CZ-HC0.1 nanomaterials.

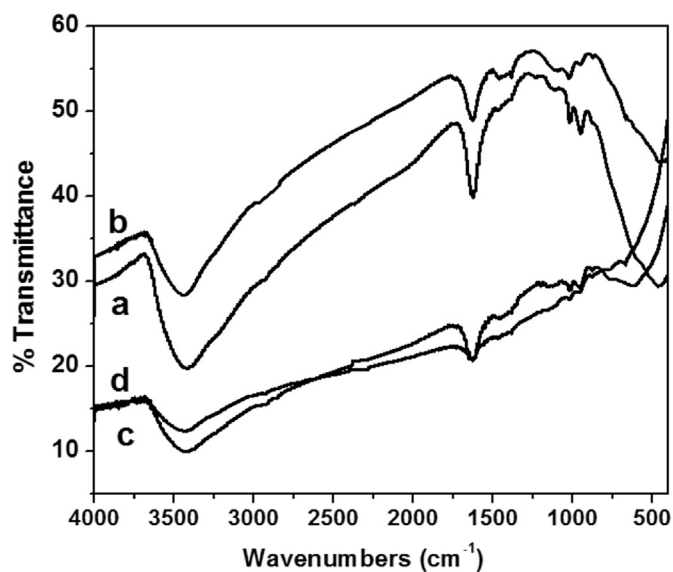


Fig. 3. FT-IR spectra of (a) CZ-H213, (b) CZ-HC0.1, (c) CZ-HT0.1 and (d) CZ-HS0.1 nanomaterials.

resulted in a decrease in the surface area of samples. It must be pointed out that the S_{BET} value of the mesoporous CZ-HC0.6 and CZ-HT0.6 catalysts was higher than that of CZ-HS0.1 and CZ-H213 catalysts which have the smallest value of the S_{BET} . It was reported that increasing the surfactant content resulted in an increase in the particle size [39]. This can be explained by that increasing surfactant content at constant water content led to an increase in the number of the reaction pools (water in oil droplets). Consequently, more sites were available for nucleation of the particles, which were expected to yield smaller particles [40]. However, the increased number of droplets, as increasing the

concentration of the surfactant, that led to a high rate of collisions among these droplets (shorter droplet mean-free path), hence, increased the probability of agglomeration of nanoparticles upon centrifugal separation as well as decreased the surface area of samples.

The corresponding pore size distributions of all synthesized mesoporous catalysts (Fig. 4B) showed multimodal distributions in the low mesoporous region with average pore diameters from 2 nm to 6 nm. Interestingly, a broad pore size distribution was observed for all nanomaterials showing the usual pore distribution of an amorphous material. The results of the textural characterization were in agreement with the XRD and HR-TEM results discussed earlier. Finally, it was noticeable that the surface area and pore volume of the mesoporous catalysts synthesized using non-ionic surfactant (Triton X-100) and cationic surfactant (CTAB) were much higher than those of anionic surfactant (SDS) or surfactant-free (CZ-H213), demonstrating remarkable role of CTAB and Triton X-100 surfactants, which makes them attractive in the field of catalysis.

3.2. Optical properties

UV–vis diffuse reflectance spectra (DRS) of the mesoporous $0.25\text{Cr}_2\text{O}_3\text{--}0.75\text{ZrO}_2$ catalysts synthesized using SDS, CTAB and Triton X-100 as surfactants with two different contents were represented in Fig. 5A. The optical spectra of all the nanomaterials consist of two broad peaks one in the range 290–350 nm and the another peak at 450–550 nm. The absorption peak centered at 330 nm corresponding to the $\text{O}^{2-} (2p) \rightarrow \text{Zr}^{4+} (4d)$ charge transfer transition [27,41]. Nevertheless, the absorption peak centered at 520 nm was assigned to the d–d transition ${}^2\text{A}_{2g} - {}^2\text{T}_{1g}, {}^2\text{E}_{2g}$, characteristic of Cr(III) ions in a distorted octahedral coordination [42].

The optical band-gap energy (E_g) of the mesoporous catalysts was given by an equation as [43]:

$$\alpha h\nu = A (h\nu - E_g)^{1/2} \quad (1)$$

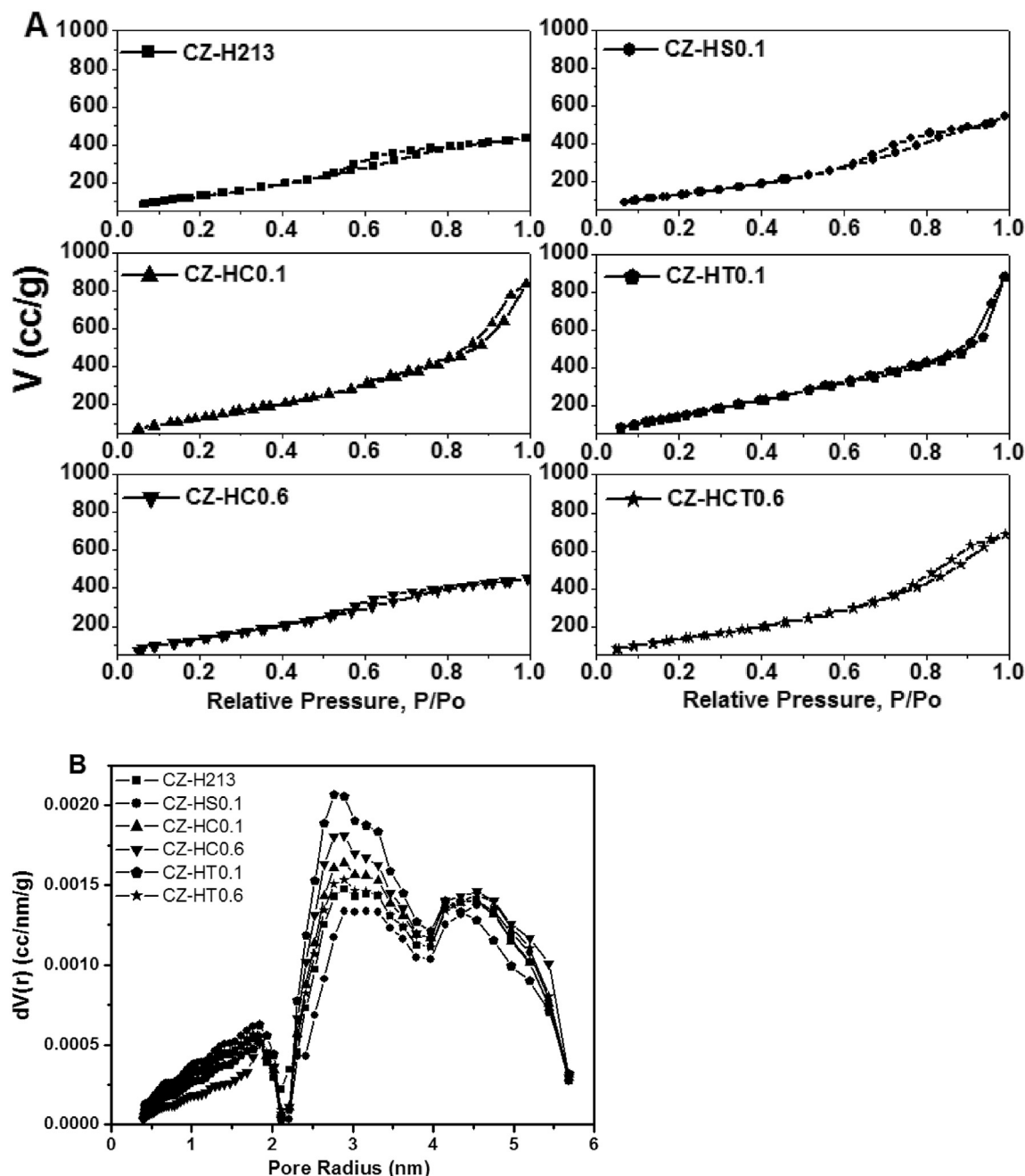


Fig. 4. (A) Nitrogen adsorption–desorption isotherms and (B) pore size distribution of nanomaterials synthesized in the absence and presence of surfactants (SDS, CTAB and Triton X-100).

where $\alpha = 2.303 \times \ln(I_0/I)/t$, here $\ln(I_0/I)$, absorbance and t , thickness of the sample. A is a constant for a direct transition and $h\nu$ is photon energy of the incident radiation. The extrapolation curve of the $(\alpha h\nu)^2$ vs. $(h\nu)$ plot was shown in Fig. 5B. Moreover, the optical band-gap energy (E_g) values for all nanomaterials ranged from 3.31 to 3.50 eV corresponding to ZrO_2 and another one constant at 2.20 eV for Cr_2O_3 were tabulated in Table 1. The sequence of the E_g values was found to be as follows: CZ-HC0.1 (3.50 eV) > CZ-HT0.1 (3.48 eV) > CZ-HC0.6 (3.44 eV) > CZ-HT0.6 (3.40 eV) > CZ-H213 (3.32 eV) > CZ-HS0.1 (3.31 eV). It was noteworthy that the band-gap energy of the mesoporous catalysts synthesized using cationic surfactant (CTAB) and non-ionic surfactant (Triton X-100) with two different concentrations was larger than those of anionic surfactant

(SDS) or surfactant-free (CZ-H213). Interestingly, the optical property test indicates that the absorption peak of the nanomaterials shifts towards the short wavelength by changing the various surfactants. And the blue shift phenomenon might be ascribed to the quantum confinement effect [43,44]. The results of the optical properties are in agreement with the XRD, HR-TEM and the textural characterization discussed earlier.

3.3. NH_3 -temperature programmed desorption (NH_3 -TPD)

The ammonia adsorption–desorption technique was carried out to determine the strength of acid sites present on the catalyst surface together with total acidity. Fig. 6 shows the NH_3 -TPD

Table 1
Physicochemical properties of mesoporous 0.25Cr₂O₃–0.75ZrO₂ surfactant-assisted and surfactant-free catalysts.

Catalyst	S _{BET} (m ² /g)	V _p (cm ³ /g) ^a	Average pore diameter (nm) ^b	T _{max} -NH ₃ (°C) ^c	TPD acid sites distribution			Total acidity (μmol/g)	Density of acidic site (μmol/m ²) ^d	Band-gap energy (ev)	
					Weak	Medium	Strong			Cr ₂ O ₃	ZrO ₂
CZ-H213	526.6	0.65	4.8	84, 295, 450	84	10	2	96	0.182	2.20	3.32
CZ-HS0.1	511.6	0.81	5.9	77, 600	66	–	13	79	0.154	2.20	3.31
CZ-HC0.1	588.4	1.25	2.6	86, 305, 460	90	49	4	143	0.243	2.20	3.50
CZ-HC0.6	569.9	0.68	4.6	–	–	–	–	–	–	2.20	3.44
CZ-HT0.1	646.4	1.32	3.3	86, 680	61	–	98	159	0.246	2.20	3.48
CZ-HT0.6	557.6	1.03	4.1	–	–	–	–	–	–	2.20	3.40

^a Pore volume.

^b Average pore diameter obtained from BJH method.

^c Temperature at desorption peak maximum.

^d Density of acidic site = amount of acidic site/BET.

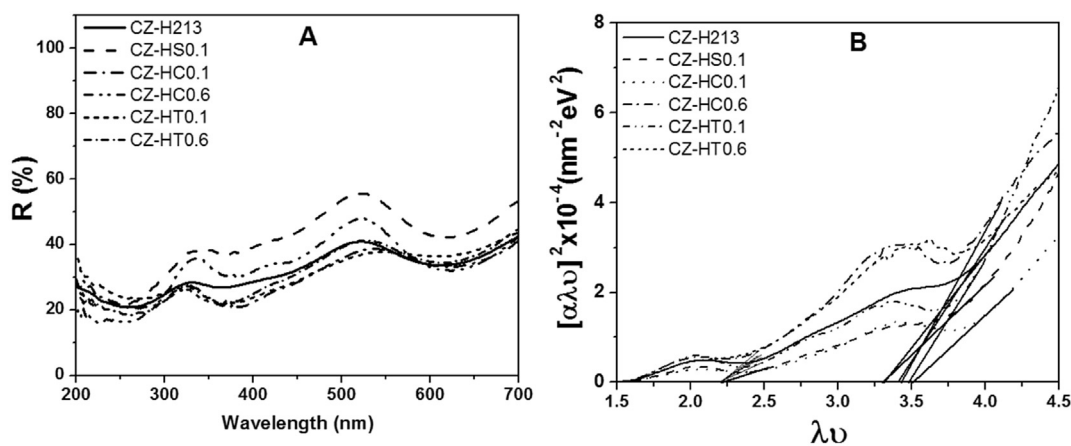


Fig. 5. (A) UV-vis/DR spectra and (B) Plot of $(\alpha\lambda\nu)^2$ vs. $(h\nu)$ of nanomaterials synthesized in the absence and presence of surfactants (SDS, CTAB and Triton X-100).

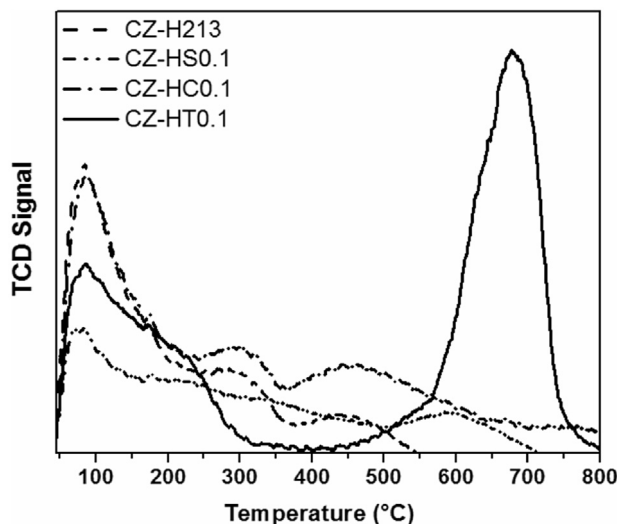


Fig. 6. NH₃-TPD profiles of CZ-H213, CZ-HS0.1, CZ-HC0.1 and CZ-HT0.1 catalysts.

profiles for the as-prepared mesoporous CZ-H213, CZ-HS0.1, CZ-HC0.1 and CZ-HT0.1 catalysts. The total acidity and the density of acid sites (i.e. the amount of acid sites per BET specific surface area) of the samples were presented in Table 1. The strength of acidic sites was determined on the basis of NH₃ desorption temperature [38]. Ammonia from weak acidic sites desorbs at < 200 °C, from moderately acidic sites it desorbs at 200–350 °C and from strongly

acidic sites it desorb at > 350 °C [45]. The NH₃-TPD profiles of CZ-H213, CZ-HS0.1, CZ-HC0.1 and CZ-HT0.1 nanomaterials were distributed over the temperature from 50 to 800 °C which indicate that the acid strength was distributed from weak to strong uniformly. However, the total acidity of CZ-H213, CZ-HS0.1, CZ-HC0.1 and CZ-HT0.1 catalysts were respectively 96, 79, 143 and 159 μmol/g evidencing that the non-ionic and cationic surfactants enhanced the amount of acidic sites. In other words, the CZ-HT0.1 catalyst had the highest acidity then this was followed by CZ-HC0.1 catalyst and the CZ-HS0.1 catalyst had the lowest acidity (c.f. Table 1). Furthermore, the density of acid sites for all synthesized nanomaterials obeys the same sequence of the total acidity as represented in Table 1. Based on the above results, the non-ionic surfactant-assisted catalyst (CZ-HT0.1) not only exhibited the highest acidity but also had the largest number of strong acid sites with very high signal intensity among all catalysts. Therefore, it could be said that the presence of non-ionic surfactant (TX-100) increased the number of strong acidic sites similar to the enhancement in surface area (Table 1) [46]. Generally, it was reported that the surfaces of metal oxides were composed of cations (Mⁿ⁺) and oxide ions (O²⁻). They were terminated by OH-groups at low temperatures. Lewis acid sites, i.e. unsaturated cations (Mⁿ⁺), were formed during thermal dehydroxylation of the metal oxides [47,48]. Furthermore, it was reported that the Brønsted acid sites corresponds to NH₃ desorption temperatures higher than 400 °C [49,50]. In other words, the addition of non-ionic surfactant (TX-100) increased the number of Brønsted acidic sites on the catalyst surface. Finally, the nature of acid sites is very important property of these catalysts.

3.4. Effect of changing surfactant type and concentration on the catalytic activity

Ethanol oxidation was measured at reaction temperatures from 150 to 400 °C over the mesoporous surfactant-assisted and surfactant-free catalysts. In addition to the ethylene (C_2H_4), other by-products like diethyl ether (DEE) (less than 15%), acetaldehyde (CH_3CHO) (less than 10%) and acetone (CH_3COCH_3) (less than 2%) were detected in ethanol oxidation. Fig. 7 (A–E) represents the total ethanol conversion (TC %) and yields of C_2H_4 , DEE, CH_3CHO and

CH_3COCH_3 versus the reaction temperature for all the as-prepared mesoporous catalysts, respectively. It was pointed out that the total ethanol conversion and C_2H_4 yield were progressively increased with the rise in reaction temperature as shown in Fig. 7 (A&B), respectively. In the low reaction temperature region (150–225 °C), all the mesoporous catalysts had similar ethanol conversion and C_2H_4 yield. However, the prepared catalysts exhibited different activities by increasing the reaction temperature from 250 to 400 °C. Generally, the non-ionic and cationic surfactant assisted catalysts with two different contents exhibited higher catalytic

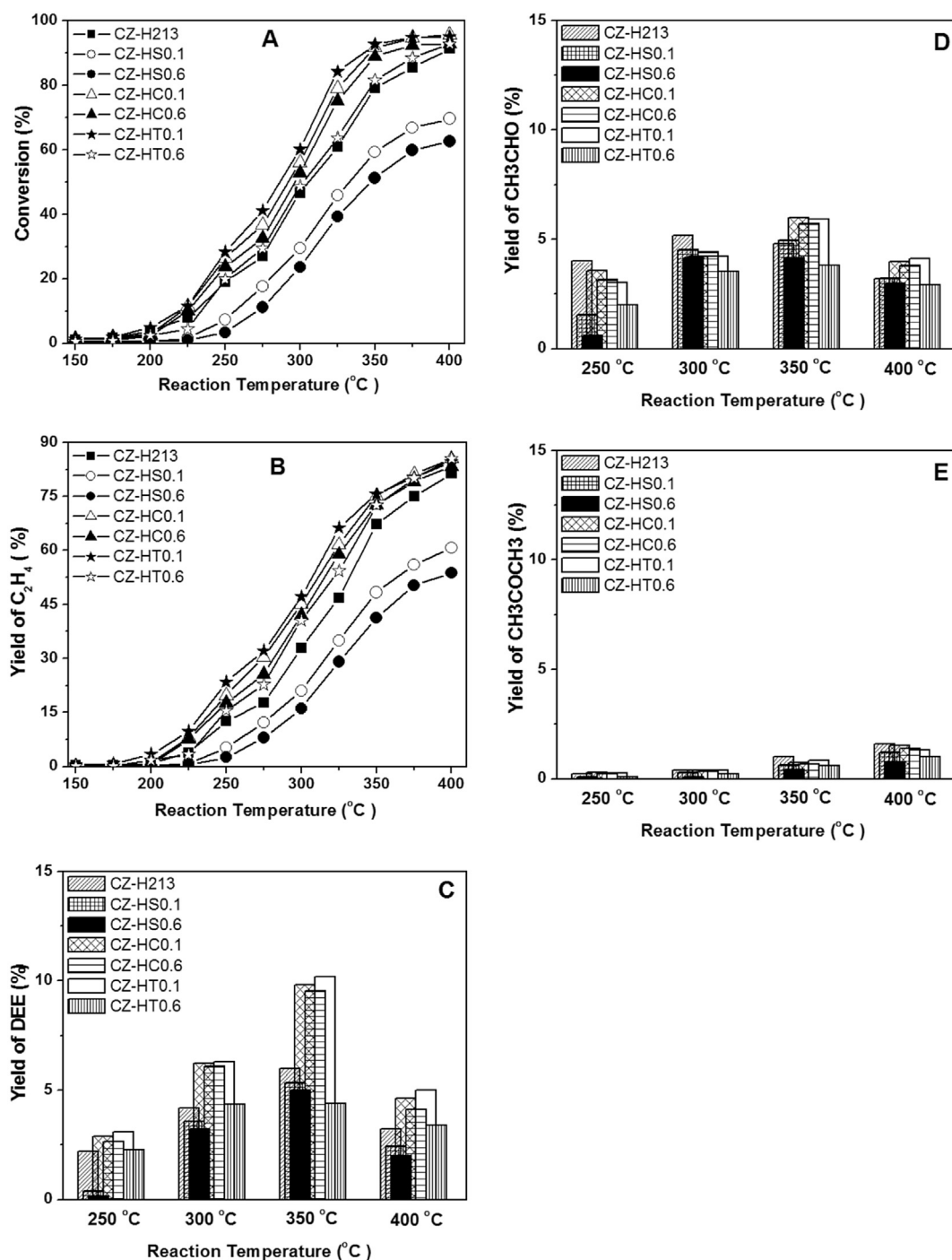


Fig. 7. (A) The total ethanol conversion (TC %), (B) ethylene yield, (C) diethyl ether yield, (D) acetaldehyde yield and (E) acetone yield of nanomaterials synthesized in the absence and presence of surfactants (SDS, CTAB and Triton X-100) as a function of the reaction temperature.

activities than the surfactant-free or anionic assisted surfactant catalysts. Specially, the CZ-HT0.1 catalyst exhibited the highest catalytic activity and the CZ-HC0.1 catalyst exhibited the secondly highest catalytic activity. Additionally, the activity sequence of all nanomaterials was as follows: CZ-HT0.1 > CZ-HC0.1 > CZ-HC0.6 > CZ-HT0.6 > CZ-H213 > CZ-HS0.1 > CZ-HS0.6. That is to say, the total ethanol conversion (TC %) of the synthesized catalysts measured at 325 °C decreased as 84.2% > 79.1% > 75.2% > 63.6% > 60.9% > 45.8% > 39.2%, respectively. Furthermore, the C₂H₄ yield for all synthesized nanomaterials obeys the same sequence of the total ethanol conversion as represented in Fig. 7 (A&B). It was noteworthy that increasing the surfactant content led to a limited decrease in the catalytic activity of catalysts. Interestingly, the total ethanol conversion and C₂H₄ yield of the mesoporous CZ-HC0.6 and CZ-HT0.6 catalysts were higher than that of surfactant-free or anionic assisted surfactant catalysts.

Increasing the reaction temperature, the DEE yield increases reached the highest values at 350 °C then decreases by increasing the reaction temperature as shown in Fig. 7C. Otherwise, the DEE yield for all synthesized nanomaterials obeys the same sequence of the C₂H₄ yield as represented in Fig. 7B. The yield of CH₃CHO increased slightly as the reaction temperature increased reached the highest values at 350 °C then decreased by increasing the reaction temperature as displayed in Fig. 7D. Further, the acetone yield increased as reaction temperature rose as presented in Fig. 7E. These results were in line with the reaction mechanism involving acetaldehyde as the main intermediate of the acetone synthesis via aldol condensation of acetaldehyde [27]. Additionally, the yields of CH₃CHO and CH₃COCH₃ were very similar for all synthesized catalysts.

It has been widely acknowledged that catalytic activity can be influenced and enhanced by a number of factors [51,52], and within this study it has been found that a combination of factors, particularly surface, morphology, optical and acidity properties have caused significant changes to the ethanol oxidation for the as-prepared mesoporous catalysts. Therefore, the CZ-HT0.1 catalyst prepared using Triton X-100 as a non-ionic surfactant exhibited the highest ethanol conversion and the CZ-HC0.1 catalyst prepared using CTAB as a cationic surfactant exhibited the secondly highest ethanol conversion. This influence has been attributed to acquiring the highest surface area (646.4 m²/g and 588.4 m²/g, respectively), the highest pore volume (1.32 cm³/g and 1.25 cm³/g respectively), the lowest particle size (1.3 nm and 0.9 nm, respectively), the largest optical band-gap energy (3.48 eV and 3.50 eV, respectively) and the highest total acidity (159 and 143 μmol/g, respectively) among all current mesoporous catalysts. It clearly indicated that the conversion of ethanol slightly decreased by increasing the surfactant concentration. This influence can be explained that those catalysts had lower surface area, smaller pore volume, lower optical band-gap energy and smaller total acidity than the same catalysts with low surfactant concentration. Obviously, the lowest catalytic activity was observed with the catalysts synthesized using anionic surfactant (SDS) which might be due to acquiring the lowest surface area, the largest particle size, the lowest optical band-gap energy and the smallest total acidity.

It was reported that the presence of acidic sites on catalyst surface were believed to be an important factor for influencing the catalytic performance in the oxidation of alcohols [46,53,54]. It was pointed out that the non-ionic and cationic surfactant assisted catalysts with two different concentrations exhibited higher C₂H₄ and DEE yields than the surfactant-free or anionic assisted surfactant catalysts as shown in Fig. 7 (B&C). Further, the C₂H₄ and DEE yields significantly increased with the total acidity and density of acid sites on the catalyst surface [46]. Interestingly, the CZ-HT0.1

catalyst presented the biggest C₂H₄ and DEE yields most probably because of the presence of the largest number of strong acid sites on its surface as understood from the highest temperature of ammonia desorption in Table 1 [46,55]. Additionally, the CZ-HC0.1 catalyst demonstrated the secondly biggest C₂H₄ and DEE yields. This was most probably attributable to the larger density and strength of acidic sites (here predominated by the weak and medium acid types) than the other catalysts. Moreover, the C₂H₄ and DEE yields on the surfactant-free or anionic assisted surfactant catalysts were low, which might be due to the presence of small number and density of acid sites. One may conclude from these observations that the Triton X-100 and CTAB surfactants play an important role in increasing the surface area, pore volume, optical band-gap energy and total acidity of the catalyst which it is related to the improvement of catalytic activity.

3.5. Proposed synthesis reaction mechanism

Surfactants were surface active agents having both hydrophobic and hydrophilic properties [56]. They can be classified as anionic, cationic, zwitter ionic and non-ionic depending on the surface charge character of the hydrophilic group as shown in Fig. 8 [57].

Two important features which characterize surfactants were namely adsorption at interface and self-accumulation into supra-molecular structures. The adsorption of surfactants onto inorganic and organic surfaces usually depends on the chemical characteristics of particles, surfactant molecules and solvent [58]. Thus, the cationic surfactants adsorb onto the negatively charged surface through its positively charged hydrophilic head keeping its hydrophobic end away from the surface. So, they constitute a new surface that repels polar solvents including water. A hydrophobic surface is also constituted when anionic surfactants bind to a positively charged surface. Depending upon the nature of surfaces, non-ionic surfactants can adsorb onto the surface with either the hydrophilic or the hydrophobic group oriented toward the surface. Zwitter ionic surfactants owing to having both positive and negative charges can adsorb onto both a negatively charged and positively charged surface without significantly changing the charge profile of the surface [59]. Once the adsorption of surfactant molecules on particle surfaces is established, self-organization of the surfactant into micelles (aggregative structures of surfactants) is expected to occur above a critical micelle concentration (CMC). The CMC is the concentration of surfactants in free solution in equilibrium with surfactants in aggregated form [58].

In the present study, CTAB was used as a cationic surfactant

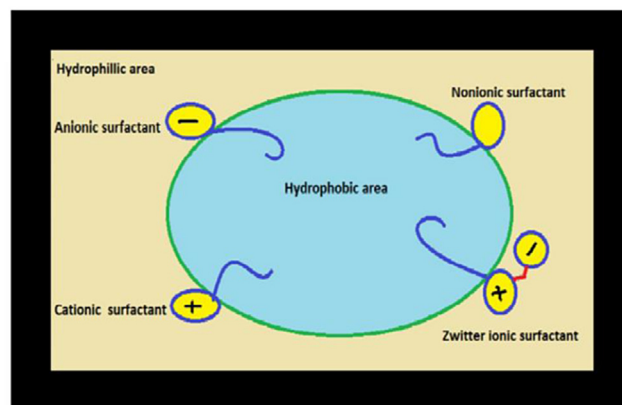


Fig. 8. Schematic representation of various surfactants. Taken from Ref. [57].

which ionizes completely in water. At the beginning of CTAB-assisted hydrothermal process, ion-pairs between $\text{Cr}(\text{OH})_3^-$ – $\text{ZrO}(\text{OH})_4^{2-}$ and CTA^+ could interact electrostatically to produce micelle-forming agents which were adsorbed on the surface [60]. On the other hand, anionic surfactant (SDS) was dissolved in water to give DS^- anion. Therefore, the positive chromium and zirconium ions interacted with the hydrophilic head of DS^- via coulombic attraction to produce micelle-forming agents which were adsorbed on the surface [34]. Furthermore, non-ionic surfactant (TX-100) was another type which does not ionize in water, because its hydrophilic component was non-dissociable like alcohol or ether. Thus, the metal hydroxide precursor interacted with TX-100 through hydrogen bonding or van der Waals forces to produce micelle-forming agents which were adsorbed on the surface [31,61].

Generally, because of this adsorption, the surface energy of binary oxide nuclei decreases, resulting in active sites being generated on the surface [30,62]. In addition, the surfactant molecules adhere to the surface of the final nanoparticles serve as a protective layer to prevent these particles from being agglomerated and therefore decreasing the particle size of the nanoparticles [60]. Finally, the surfactant molecules can be removed by washing with bi-distilled water as confirmed by FT-IR (Fig. 3). According to above results, the smallest sized and well-dispersed $0.25\text{Cr}_2\text{O}_3$ – 0.75ZrO_2 nanomaterials were obtained successfully with cationic surfactant (CTAB) and non-ionic surfactant (TX-100) assisted by the hydrothermal process.

4. Conclusions

In conclusion, novel mesoporous $0.25\text{Cr}_2\text{O}_3$ – 0.75ZrO_2 nanomaterials with three different types of surfactants were synthesized via hydrothermal method. The physicochemical properties of the catalysts were studied by the XRD, HR-TEM, FT-IR, BET, UV–vis/DR, NH_3 -TPD techniques. The obtained results indicated that the catalysts prepared with non-ionic (Triton X-100) and cationic (CTAB) surfactants are the best, in terms of particle size, surface area, optical, acidic and catalytic properties.

Acknowledgements

I would like to thank Dr. M. Saif (Ain Shams University, Egypt) for her lab facilities and Dr. Aïcha Mbarek (Clermont Université, France and Université de Sfax, Tunisie) for the XRD measurement.

References

- [1] M. Fernández-García, J.A. Rodríguez, *Encyclopedia of Inorganic and Bioinorganic Chemistry: Metal Oxide Nanoparticles*, John Wiley & Sons, Ltd, New York, NY, USA, 2011, pp. pp.1–3.
- [2] J. Ying, T. Zhang, M. Tang, Metal oxide nanomaterial QNAR models: available structural descriptors and understanding of toxicity mechanisms, *Nanomaterials* 5 (2015) 1620–1637.
- [3] S. Farhadi, K. Pourzare, S. Sadeghinejad, Simple preparation of ferromagnetic Co_3O_4 nanoparticles by thermal dissociation of the $[\text{Co}^{\text{II}}(\text{NH}_3)_6](\text{NO}_3)_2$ complex at low temperature, *J. Nanostruct. Chem.* 3 (2013) 16–22.
- [4] M. Raghasudha, D. Ravinder, P. Veerasomaiah, Magnetic properties of Cr-substituted Co-ferrite nanoparticles synthesized by citrate-gel auto combustion method, *J. Nanostruct. Chem.* 3 (2013) 63–68.
- [5] C. Ramesh, K.M. Kumar, M. Senthil, V. Ragnathan, Antibacterial activity of Cr_2O_3 nanoparticles against *E.coli*; Reduction of chromate ions by *Arachis hypogaea leaves*, *Arch. Appl. Sci. Res.* 4 (2012) 1894–1900.
- [6] H.L. Zhang, S.T. Liang, M.T. Luo, M.G. Ma, P.P. Fan, H.B. Xu, P. Li, Y. Zhang, Preparation and color performance control of Cr_2O_3 green pigment through thermal decomposition of chromium hydroxide precursor, *Mater. Lett.* 117 (2014) 244–247.
- [7] N.-N. Li, G.-I. Li, H.-D. Wang, J.-J. Kang, T.-S. Dong, H.-J. Wang, Influence of TiO_2 content on the mechanical and tribological properties of Cr_2O_3 -based coating, *Mater. Des.* 88 (2015) 906–914.
- [8] S. Park, S. Kim, G.-J. Sun, S. Choi, S. Lee, C. Lee, Ethanol sensing properties of networked In_2O_3 nanorods decorated with Cr_2O_3 -nanoparticles, *Ceram. Int.* 41 (2015) 9823–9827.
- [9] Y. Gan, Y. Lai, Z. Zhang, W. Chen, K. Du, J. Li, Hierarchical Cr_2O_3 @OPC composites with octahedral shape for rechargeable nonaqueous lithium-oxygen batteries, *J. Alloys Comp.* 665 (2016) 365–372.
- [10] H.R. Mahmoud, Novel mesoporous Gd^{3+} doped Cr_2O_3 nanomaterials: synthesis, characterization, catalytic and antitumor applications, *Adv. Powder Technol.* (2016), <http://dx.doi.org/10.1016/j.apt.2016.05.003>.
- [11] S. Khamlich, M. Maaza, Cr/ α - Cr_2O_3 monodispersed meso-spherical particles for mid-temperature solar absorber application, *Energy Procedia* 68 (2015) 31–36.
- [12] P.M. Perillo, D.F. Rodríguez, Anodization growth of self-organized ZrO_2 nanotubes on zircaloy-4, *Eval. Photocatalytic Activity Revista Matéria* 20 (2015) 627–635.
- [13] K. Shimizu, I. Chinzei, H. Nishiyama, S. Kakimoto, S. Sugaya, H. Yokoi, A. Satsuma, Hydrogen sensor based on WO_3 subnano clusters and Pt co-loaded on ZrO_2 , *Sens. Actuators B* 134 (2008) 618–624.
- [14] A.O. de Souza, F.F. Ivashita, V. Biondo, A. Paesano, D.H. Mosca, Structural and magnetic properties of iron doped ZrO_2 , *J. Alloys Comp.* 680 (2016) 701–710.
- [15] R. Kitazawa, H. Kakisawa, Y. Kagawa, Anisotropic TGO morphology and stress distribution in EB-PVD Y_2O_3 - ZrO_2 thermal barrier coating after in-phase thermo-mechanical test, *Surf. Coat. Technol.* 238 (2014) 68–74.
- [16] G.I.V. Carbajal, J.L.R. Galicia, J.C.R. Angeles, J.L. Cuevas, C.H.G. Chavarria, Microstructure and mechanical behavior of alumina-zirconia-mullite refractory materials, *Ceram. Int.* 38 (2012) 1617–1625.
- [17] H.R. Mahmoud, Highly dispersed Cr_2O_3 – ZrO_2 binary oxide nanomaterials as novel catalysts for ethanol conversion, *J. Mol. Catal. A* 392 (2014) 216–222.
- [18] N.R. Park, C.G. Song, I.J. Shon, Fast low-temperature consolidation of a nano-structured 2Ti – ZrO_2 composite for biomedical applications, *Ceram. Int.* 40 (2014) 6311–6317.
- [19] H. Ding, M. Wan, Y. Wei, Controlling the diameter of polyaniline nanofibers by adjusting the oxidant redox potential, *Adv. Mater.* 19 (2007) 465–469.
- [20] A.S. Vanetsev, E.V. Samsonova, O.M. Gaitko, K. Keevend, A.V. Popov, U. Mäeorg, H. Mändar, I. Sildos, YuV. Orlovskii, Phase composition and morphology of nanoparticles of yttrium orthophosphates synthesized by microwave-hydrothermal treatment: the influence of synthetic conditions, *J. Alloys Comp.* 639 (2015) 415–421.
- [21] Y. Dai, J. Li, G. Yan, G. Xu, Q. Xue, F. Kang, Preparation of the cactus-like porous manganese oxide assisted with surfactant sodium dodecyl sulfate for supercapacitors, *J. Alloys Comp.* 621 (2015) 86–92.
- [22] B. Zou, S. Gong, Y. Wang, X. Liu, Tungsten oxide and polyaniline composite fabricated by surfactant-templated electrodeposition and its use in supercapacitors, *J. Nanomater.* (2014) 1–9, <http://dx.doi.org/10.1155/2014/813120>.
- [23] A. Barrabino, Synthesis of mesoporous silica particles with control of both particle diameter and particle size, 2011. Göteborg, Sweden.
- [24] M.M. Khalaf, H.G. Ibrahimov, E.H. Ismailov, Nanostructured materials: importance, synthesis and characterization—a review, *Chem. J.* 2 (2012) 118–125.
- [25] S. Arenamart, W. Trakarnpruk, Ethanol conversion to ethylene using metal-mordenite catalysts, *Int. J. Appl. Sci. Eng.* 4 (2006) 21–32.
- [26] M. Mokhtar, S.N. Basahel, T.T. Ali, Ethanol to hydrocarbons using silver substituted polyoxometalates: physicochemical and catalytic study, *J. Ind. Eng. Chem.* 20 (2014) 46–53.
- [27] H.R. Mahmoud, Effect of hydrothermal treatment on catalytic activity of amorphous mesoporous Cr_2O_3 – ZrO_2 nanomaterials for ethanol oxidation, *Mater. Chem. Phys.* 162 (2015) 50–58.
- [28] Y. Gong, H. Chen, Y. Chen, X. Cui, Y. Zhu, X. Zhou, J. Shi, A Cu/Mn co-loaded mesoporous ZrO_2 – TiO_2 composite and its CO catalytic oxidation property, *Microporous Mesoporous Mater.* 173 (2013) 112–120.
- [29] B. Neppolian, Q. Wang, H. Yamashita, H. Choi, Synthesis and characterization of ZrO_2 – TiO_2 binary oxide semiconductor nanoparticles: application and interparticle electron transfer process, *Appl. Catal. A* 333 (2007) 264–271.
- [30] A.P. de Moura, R.C. Lima, M.L. Moreira, D.P. Volanti, J.W.M. Espinosa, M.O. Orlandi, P.S. Pizani, J.A. Varela, E. Longo, ZnO architectures synthesized by a microwave-assisted hydrothermal method and their photoluminescence properties, *Solid State Ion* 181 (2010) 775–780.
- [31] M. Kooti, L. Matouri, A facile and mild method for synthesis of nickel oxide nanoparticles in the presence of various surfactants, *RRJMS* 2 (2014) 37–42.
- [32] S.A. El-Molla, H.R. Mahmoud, Synthesis, textural and catalytic properties of nanosized Fe_2O_3 /MgO system, *Mater. Res. Bull.* 48 (2013) 4105–4111.
- [33] X. Ye, S. Cai, C. Zheng, X. Xiao, N. Hua, Y. Huang, SiO_2 /TiO₂/Ag multilayered microspheres: preparation, characterization, and enhanced infrared radiation property, *Appl. Surf. Sci.* 345 (2015) 279–285.
- [34] X. Sang, L. Zhang, H. Wang, D. He, L. Deng, S. Huang, J. Wang, Y. Luo, Influence of synthetic parameters on structural and catalytic properties of sulfated zirconia nanoparticles prepared by employing sulfate-containing anion surfactants via one-step route, *Powder Technol.* 253 (2014) 590–595.
- [35] G. Pandey, S. Dixit, A.K. Shrivastava, Role of additives; sodium dodecyl sulphate and manganese chloride on morphology of $\text{Zn}_{1-x}\text{Mn}_x\text{O}$ nanoparticles and their photoluminescence properties, *Mater. Chem. Phys.* 147 (2014) 423–432.
- [36] X. Wang, J. Liu, H. Du, J.D. Miller, States of adsorbed dodecyl amine and water at a silica surface as revealed by vibrational spectroscopy, *Langmuir* (2010) 3407–3414.
- [37] H. Adelkhani, M. Ghaemi, M. Ruzbehani, Evaluation of the porosity and the

- nano- structure morphology of MnO₂ prepared by pulse current electrodeposition, *Int. J. Electrochem. Sci.* 6 (2011) 123–135.
- [38] S. Badoga, R.V. Sharma, A.K. Dalai, J. Adjaye, Synthesis and characterization of mesoporous aluminas with different pore sizes: application in NiMo supported catalyst for hydrotreating of heavy gas oil, *Appl. Catal. A* 489 (2015) 86–97.
- [39] M.F.R. Fouda, M.B. El-Kholy, S.A. Moustafa, A.I. Hussien, M.A. Wahba, M.F. El-Shahat, Synthesis and characterization of nanosized Fe₂O₃ pigments, *Int. J. Inorg. Chem.* (2012) 1–9, <http://dx.doi.org/10.1155/2012/989281>.
- [40] M.R. Cornell, U. Schwertmann, *The Iron Oxides: Structure, Properties, Reactions, Occurrences and Uses*, second ed., Wiley-VCH, Weinheim, Germany, 2003.
- [41] N.C.S. Selvam, A. Manikandan, L.J. Kennedy, J.J. Vijaya, Comparative investigation of zirconium oxide (ZrO₂) nano and microstructures for structural, optical and photocatalytic properties, *J. Colloid Interface Sci.* 389 (2013) 91–98.
- [42] P.M.C. Zapata, M.S. Nazzarro, M.L. Parentis, E.E. Gonzo, N.A. Bonini, Effect of hydrothermal treatment on Cr-SiO₂ mesoporous materials, *Chem. Eng. Sci.* 101 (2013) 374–381.
- [43] J. Gajendran, V. Rajendran, Different surfactants assisted on the synthesis of SnO₂ nanoparticles and their characterization, *Int. J. Mater. Biomater. Appl.* 2 (2012) 37–40.
- [44] K. Anandan, V. Rajendran, Sheet, spherical and plate-like chromium sesquioxide (Cr₂O₃) nanostructures synthesized via ionic surfactants assisted facile precipitation method, *Mater. Lett.* 146 (2015) 99–102.
- [45] S. Badoga, A.K. Dalai, J. Adjaye, Y. Hu, Combined effects of EDTA and heteroatoms (Ti, Zr, and Al) on catalytic activity of SBA-15 supported NiMo catalyst for hydrotreating of heavy gas oil, *Ind. Eng. Chem. Res.* 53 (2014) 2137–2156.
- [46] S. Narayanan, J.J. Vijaya, S. Sivasanker, L.J. Kennedy, S.K. Jesudoss, Structural, morphological and catalytic investigations on hierarchical ZSM-5 zeolite hexagonal cubes by surfactant assisted hydrothermal method, *Powder Technol.* 274 (2015) 338–348.
- [47] M.I. Zaki, M.A. Hasan, F.A. Al-Sagheer, L. Pasupulety, In situ FTIR spectra of pyridine adsorbed on SiO₂-Al₂O₃, TiO₂, ZrO₂ and CeO₂: general considerations for the identification of acid sites on surfaces of finely divided metal oxides, *Colloid Surf. A* 190 (2001) 261–274.
- [48] P. Esmailzadeh, N. Hosseinpour, A. Bahramian, Z. Fakhroueian, S. Arya, Effect of ZrO₂ nanoparticles on the interfacial behavior of surfactant solutions at air–water and n-heptane–water interfaces, *Fluid Phase Equilibria* 361 (2014) 289–295.
- [49] R. Tiwari, B.S. Rana, R. Kumar, A.K. Sinha, TiO₂-ZrO₂ binary oxides for effective hydrodesulfurization catalysts, *Open Catal. J.* 5 (2012) 39–49.
- [50] H. Zou, Y.S. Lin, Structural and surface chemical properties of sol–gel derived TiO₂-ZrO₂ oxides, *Appl. Catal. A* 265 (2004) 35–42.
- [51] A. Ananth, D.H. Gregory, Y.S. Mok, Synthesis, characterization and shape-dependent catalytic CO oxidation performance of ruthenium oxide nano-materials: influence of polymer surfactant, *Appl. Sci.* 5 (2015) 344–358.
- [52] A.-L. Anderson, R. Binions, The effect of Tween[®] surfactants in sol-gel processing for the production of TiO₂ thin films, *Coatings* 4 (2014) 796–809.
- [53] M.P. Chaudhari, S.B. Sawant, Kinetics of heterogeneous oxidation of benzyl alcohol with hydrogen peroxide, *Chem. Eng. J.* 106 (2005) 111–118.
- [54] S. Endud, K.L. Wong, Mesoporous silica MCM-48 molecular sieve modified with SnCl₂ in alkaline medium for selective oxidation of alcohol, *Microporous Mesoporous Mater.* 101 (2007) 256–263.
- [55] M. Hajheidary, M. Ghashghae, R. Karimzadeh, Olefins production from LPG via dehydrogenative cracking over three ZSM-5 catalysts, *J. Sci. Ind. Res.* 72 (2013) 760–766.
- [56] K.J. Edler, Soap and sand: construction tools for nanotechnology, *Philos. Trans. A. Math. Phys. Eng. Sci.* 362 (2004) 2635–2651.
- [57] M. Ullah, M.E. Ali, S.B. Abd Hamid, Surfactant-assisted ball milling: a novel route to novel materials with controlled nanostructure- A Review, *Rev. Adv. Mater. Sci.* 37 (2014) 1–14.
- [58] L. Vaisman, H.D. Wagner, G. Marom, The role of surfactants in dispersion of carbon nanotubes, *Adv. Colloid Interface Sci.* 128–130 (2006) 37–46.
- [59] M.J. Rosen, *Surfactants and Interfacial Phenomena*, John Wiley & Sons, Inc., Hoboken, New Jersey, 2004.
- [60] K. Anandan, V. Rajendran, Structural, optical and magnetic properties of well-dispersed NiO nanoparticles synthesized by CTAB assisted solvothermal process, *Nanosci. Nanotechnol. Int. J.* 2 (2012) 24–29.
- [61] P. Yang, D. Zhao, D.I. Margolese, B.F. Chmelka, G.D. Stucky, Generalized syntheses of large-pore mesoporous metal oxides with semicrystalline frameworks, *Nature* 396 (1998) 152–155.
- [62] H. Zhang, D.R. Yang, Y.J. Ji, X.Y. Ma, J. Xu, D.L. Que, Low temperature synthesis of flowerlike ZnO nanostructures by cetyltrimethylammonium bromide-assisted hydrothermal process, *J. Phys. Chem. B* 108 (2004) 3955–3958.